Review | Received 24 May 2026; Revised 29 June 2026; Accepted 2 July 2026; Published 17 July 2026
https://doi.org/10.55092/bm20260006

Recent advances in organic photosensitizers for tumor photodynamic therapy

Qiancheng Jin[1,†], Yuzi Huang[1,†], Wei Wang[2], Haichuang Lan[1], Shuzhang Xiao[1,*], Wen Zhang[2,*] and Peng Geng[1,2,*]

[1] Key Laboratory of Inorganic Nonmetallic Crystalline and Energy Conversion Materials, College of Materials and Chemical Engineering, China Three Gorges University, Yichang 443002, China
[2] School of Biology and Pharmaceutical Sciences, China Three Gorges University, Yichang 443002, China

† These authors contributed equally to this work.

* Correspondence authors; E-mails: shuzhangxiao@ctgu.edu.cn (S.X.); zhangwen@ctgu.edu.cn (W.Z.); gengpeng@ctgu.edu.cn (P.G.).

Highlights:

- Six major organic photosensitizer classes are compared by structure and PDT performance.
- Molecular engineering, nanodelivery, and tumor microenvironment regulation are summarized.
- AIE, NIR-II, and two-photon strategies are highlighted for precise deep-tumor PDT.

Abstract: Photodynamic therapy (PDT) has shown significant advantages in tumor treatment due to its minimally invasive nature, low toxicity, and high selectivity. This article systematically reviews the research progress of organic photosensitizers (PSs) used in tumor PDT in recent years, and classifies them into six major categories based on chemical structure: porphyrins, chlorins, phthalocyanines, fused quinones, phenothiazines, and BODIPYs. It focuses on the innovative applications of various PSs in molecular design optimization, regulation of photophysical properties, nanonization strategies, and multimodal synergistic therapy. Strategies such as targeted delivery, microenvironment modulation (e.g., hypoxia alleviation, GSH depletion, pH responsiveness), and Type I photodynamic mechanisms have significantly enhanced PDT efficacy. Combined with two-photon excitation, NIR-II window absorption, and imaging guidance, the tissue penetration and treatment precision of PSs have been improved, providing a systematic reference for the development of efficient and low-toxicity tumor PDT strategies.

Keywords: photodynamic therapy; organic photosensitizer; tumor treatment; targeted delivery; collaborative therapy

1. Introduction

Malignant tumors remain a major therapeutic challenge because of their high recurrence rates, drug resistance, and complex tumor microenvironment [1]. Conventional surgery, radiotherapy, and chemotherapy are often associated with substantial trauma, systemic toxicity, and limited therapeutic efficacy, highlighting the urgent need for novel treatment strategies that are efficient, low-toxic, and precise [2,3].

Photodynamic therapy (PDT), as a minimally invasive local treatment, relies on photosensitizers (PSs) to generate reactive oxygen species (ROS) under irradiation with light of a specific wavelength in the presence of oxygen, thereby killing tumor cells [4–6]. In addition, PDT can damage tumor vasculature and activate antitumor immune responses [7,8]. Owing to its high spatial selectivity, low systemic toxicity, and potential for multimodal combination therapy, PDT has become an important component of modern comprehensive cancer treatment [9,10].

In recent years, inorganic nanomaterials, such as TiO_2, ZnO, MoS_2, black phosphorus, and carbon-based nanomaterials, have shown unique advantages in tumor phototherapy [11]. These materials can generate ROS through mechanisms such as photoinduced electron–hole pairs and localized surface plasmon resonance. They generally exhibit strong photothermal conversion efficiency, excellent photochemical stability, facile integration with imaging contrast units, including magnetic resonance imaging (MRI), computed tomography (CT), and photoacoustic imaging, as well as the capacity to load various therapeutic agents. Therefore, they are frequently constructed as multifunctional integrated nanotheranostic platforms [12–14]. However, inorganic nanomaterials also have several non-negligible limitations, including potential toxicity caused by long-term retention *in vivo* [15], poor biodegradability, unclear metabolic pathways, unsatisfactory batch-to-batch stability, and complex surface modification procedures [16]. These factors have, to some extent, hindered their clinical translation.

To overcome the above limitations of inorganic nanophotosensitizers, organic PSs with precisely tunable structures have become a central focus in tumor PDT. Organic PSs are typically based on conjugated organic molecular cores, whose molecular skeletons can be precisely modified at the atomic level through organic synthesis. Owing to their structural diversity, broadly tunable photophysical properties, favorable biocompatibility, and relatively rapid metabolic clearance *in vivo*, organic PSs have gradually advanced toward clinical translation and cutting-edge biomedical applications [17–21]. According to their conjugated macrocyclic or chromophoric skeletons, mainstream organic PSs can be classified into six major categories: porphyrins, chlorins, phthalocyanines, fused-ring quinones, phenothiazines, and BODIPY derivatives (Figure 1). In recent years, substantial progress has been made in the molecular optimization, nanodelivery, and multimodal synergistic therapy of these six categories of organic PSs, including PDT/chemotherapy, PDT/photothermal therapy (PTT), and PDT/immunotherapy (Figure 2) [22–24]. This review systematically summarizes recent advances in organic PSs for tumor PDT. It discusses the molecular design strategies, regulation of photophysical properties, nanodelivery systems, and combined therapeutic applications of different types of PSs. In addition, emerging strategies, including hypoxia alleviation, glutathione (GSH) depletion, targeted delivery, type I PDT, and two-photon/NIR-II imaging-guided therapy, are summarized to provide theoretical references and design insights for the development of efficient, low-toxicity organic photosensitizing theranostic agents suitable for deep-seated solid tumors.

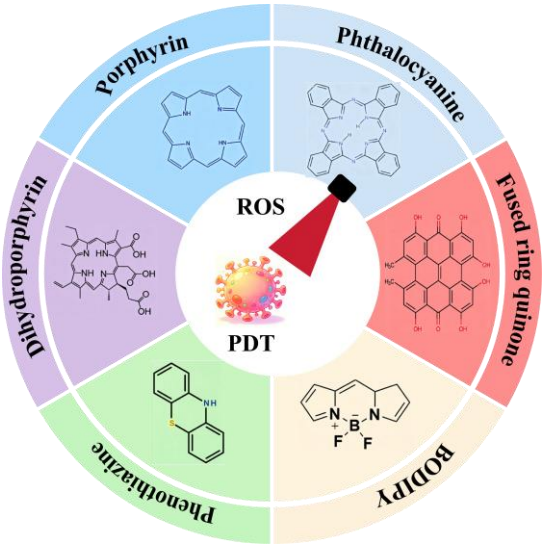

Figure 1. Six different types of organic PSs applied in tumor PDT.

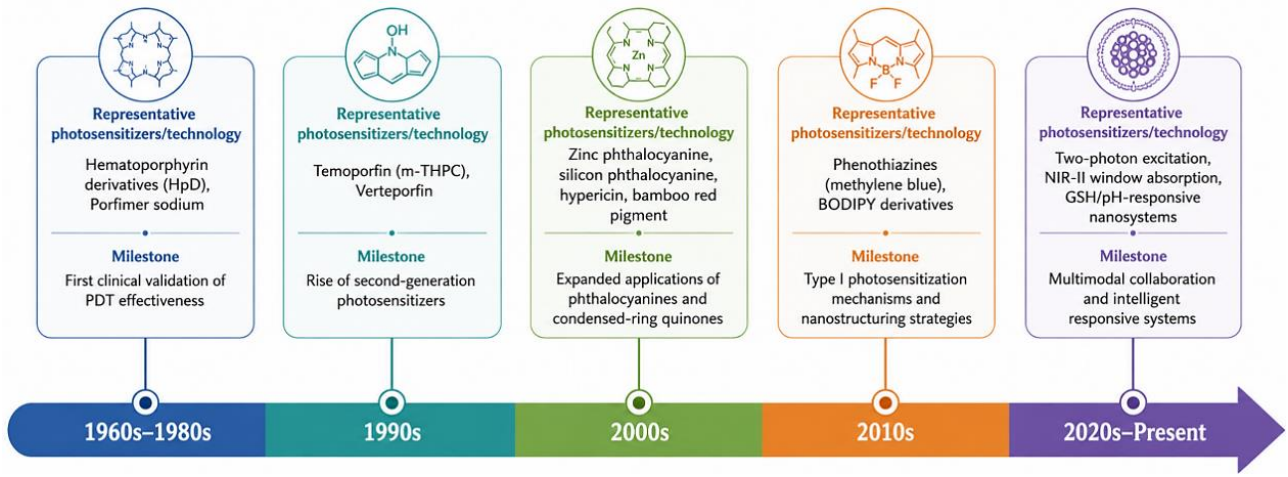

Figure 2. Milestone timeline of organic PSs for tumor PDT.

2. Classification of organic PSs

According to their chemical structures, organic PSs can be broadly divided into six major categories, each with distinct photophysical properties, mechanisms of action, and applications in tumor PDT. Porphyrins, which are based on a tetrapyrrolic macrocyclic core, such as hematoporphyrin derivatives [25,26] and porfimer sodium [27], exhibit favorable light absorption properties and stability [28]. Their partially reduced derivatives, chlorins, such as temoporfin [29] and verteporfin [30,31], display red-shifted absorption peaks in the near-infrared region, significantly improving tissue penetration and therapeutic depth [32]. Phthalocyanines, such as zinc phthalocyanine [33,34] and silicon phthalocyanine [35,36], are synthetic tetraazaporphyrin analogues with high chemical stability and absorption wavelengths extending up to 780 nm. They have shown considerable potential in multimodal PDT and combined photothermal therapy [37,38]. Fused-ring quinones, such as hypericin [39,40] and hypocrellin [41,42], are derived from natural products. Their anthraquinone or naphthoquinone structures endow them with excellent ROS-generating capacity and enable the induction of immunogenic cell death (ICD) [43]. Phenothiazines [44], represented by methylene blue (MB), possess a distinctive tricyclic “butterfly-like”

skeleton and mainly act through a type I free-radical mechanism. They are widely used in antimicrobial PDT and provide adaptability to hypoxic tumor environments for antitumor PDT [45,46]. BODIPY derivatives, namely boron-dipyrromethene compounds [47,48], as well as certain transition-metal complexes such as ruthenium and iridium complexes, can achieve tunable light absorption, optimized ROS production, and targeted delivery through flexible molecular design, offering diverse options for efficient and low-toxic tumor PDT [49].

2.1. Porphyrins

Porphyrin-based PSs feature a tetrapyrrolic macrocyclic core and are widely used in PDT because of their excellent light absorption properties and chemical stability [50]. In the application of PDT for breast cancer, Zheng's team [51] developed a Golgi-targeted immune stimulator (GA-IS) and combined it with PROTAC (Proteolysis-Targeting Chimeras) technology to degrade BRD4 (Bromodomain protein 4), thereby achieving synergistic PDT and immune regulation. The central rationale of this strategy is that Golgi targeting enables the photosensitizer to accumulate in one of the intracellular regions most sensitive to ROS. As a result, photo-generated $^1O_2$ can oxidize nearby proteins and unsaturated lipids, thereby enhancing ROS-mediated tumor cell killing. Meanwhile, PROTAC-mediated BRD4 degradation can suppress tumor cell proliferation at the epigenetic level, forming a spatiotemporally coordinated therapeutic effect with PDT. In this way, the two strategies act on different targets within the same cells, rather than merely producing a simple additive effect. This strategy significantly promoted ROS generation and inhibited tumor growth (Figure 3a). Dynamic light scattering (DLS) analysis showed that the hydrodynamic diameter of GA-IS was 204.8 nm (Figure 3b). Detection using the ROS fluorescent probe DCFH-DA revealed that the GA-Chip (+) and GA-IS (+) groups exhibited the highest intracellular ROS levels (Figure 3c), corresponding to marked tumor growth inhibition and the lowest tumor weight (Figure 3d,e). These results highlight the advantages of Golgi-targeted PDT in enhancing therapeutic efficacy. Traditional drug delivery systems, such as liposomes and albumin nanoparticles, suffer from several limitations, including low drug-loading capacity, rapid clearance by the reticuloendothelial system, and poor penetration into tumor tissues [52–54]. Although biomimetic membrane systems, such as exosomes and cell membrane-coated nanoparticles, have improved targeting efficiency, their large particle size, complex preparation procedures, and limited stability restrict cellular internalization efficiency [55]. To address these challenges, Ma's team [56] constructed porphyrin conjugates with a "hydrophobic–hydrophilic–hydrophobic" structure, termed DA-Cys-PD, in situ on tumor cell membranes through cell membrane-anchored click chemistry (Figure 3f). The design rationale of cell membrane-anchored click chemistry is to covalently attach the photosensitizer to the cell membrane surface. In this way, short-lived photo-generated ROS, particularly singlet oxygen with a diffusion distance of approximately 100–150 nm, can directly act on membrane lipids and proteins within the effective killing radius. This strategy helps avoid the loss of therapeutic efficacy caused by lysosomal sequestration or drug efflux after cellular uptake of PSs. This strategy significantly enhanced the cellular uptake and retention of PSs, enabling efficient and safe PDT for breast cancer. DLS analysis showed that the particle size of DA-Cys-PD was approximately 160 nm (Figure 3g). In the G5 group, the fluorescence signal increased over time, peaked at 8 h, and remained detectable at 24 h (Figure 3h). This group also exhibited pronounced tumor inhibition, with the lowest tumor weight of approximately 0.5 g (Figure 3i,j). For porphyrin-based PSs, recent studies indicate that subcellular targeting and

membrane-anchoring strategies can effectively improve the intracellular delivery and retention of PSs, thereby enhancing ROS generation and antitumor efficacy [57]. Compared with conventional passive delivery systems, these strategies provide more precise regulation of the interaction between PSs and tumor cells. However, many of these systems involve relatively complex molecular design or multistep preparation procedures, which may increase the difficulty of large-scale production and quality control. Therefore, future studies should further balance targeting efficiency, structural simplicity, reproducibility, and biosafety.

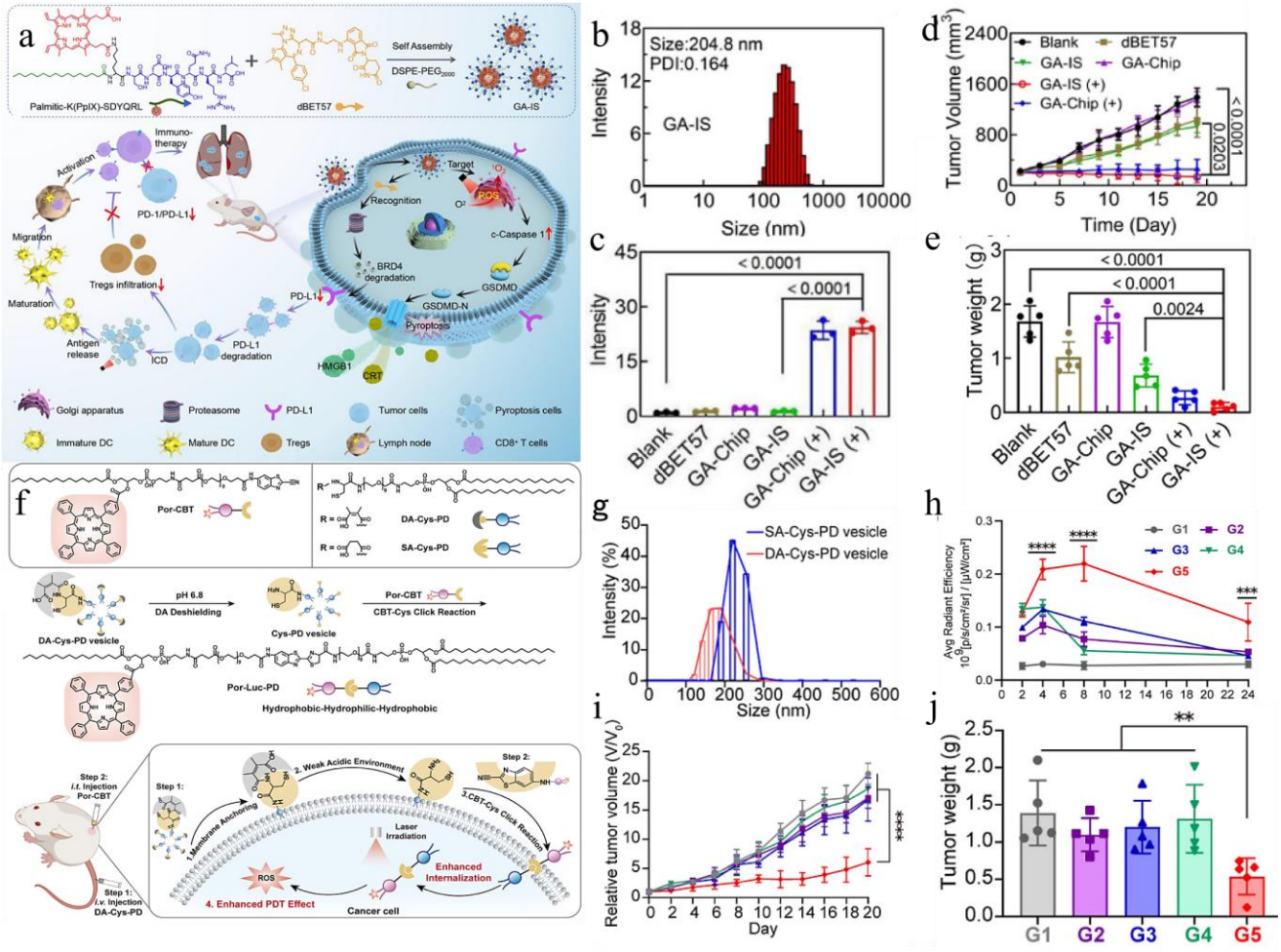

Figure 3. GA-IS and DA-Cys-PD for photodynamic therapy. **(a)** Schematic diagram of GA-IS preparation; **(b)** Hydrodynamic size of GA-IS and **(c)** ROS detection; **(d)** Tumor volume and **(e)** tumor weight changes; **(f)** Schematic diagram of Por-Luc-PD preparation; **(g)** Hydrodynamic size of SA-Cys-PD and DA-Cys-PD; **(h)** Fluorescence intensity in the tumor region of mice; **(i)** Changes in relative tumor volume over time in G1–G5 groups of mice; **(j)** Tumor weight.

2.2. Chlorins

Chlorin-based PSs are partially reduced derivatives of porphyrins, characterized by red-shifted absorption peaks in the near-infrared region and enhanced tissue penetration capability. Gu's team [58] used catalase (CAT) as a template to catalyze the decomposition of H_2O_2 for oxygen generation and to load the photosensitizer Ce6 (Chlorin e6). Meanwhile, gadolinium ions were mineralized *in situ* to construct a high-relaxivity T_1-weighted MRI imaging platform. This integrated nanoplatform, termed

Gd@CATCE6 (GCC), combined hypoxia modulation, efficient PDT, and imaging guidance within a single nanosystem (Figure 4a). The CAT template can decompose tumor-derived H_2O_2 into O_2, thereby directly supplying the key reactant required for type II photodynamic reactions, in which the triplet-state photosensitizer transfers energy to ground-state oxygen to generate $^1O_2$. In addition, the introduction of Gd^{3+} takes advantage of its MRI contrast capability, enabling therapeutic and imaging functions to be physically integrated within the same nanostructure and avoiding pharmacokinetic discrepancies caused by separate administration. DLS analysis showed that the hydrodynamic diameter of GCC was 36.6 nm (Figure 4b). Oxygen measurement results indicated that laser irradiation did not affect CAT activity, ensuring continuous oxygen supply during PDT and overcoming the therapeutic limitations of conventional PDT caused by tumor hypoxia (Figure 4c). In a 4T1 tumor-bearing mouse model, GCC achieved efficient and sustained tumor MRI enhancement, with the signal reaching its maximum at 1 h post-injection (Figure 4d). Under laser irradiation, GCC produced a tumor inhibition rate of 87.8%, which was significantly higher than that of conventional PDT using Ce6 plus laser irradiation (Figure 4e). To address the strong hydrophobicity, low tumor accumulation, and nonselective toxicity of the conventional chemotherapeutic drug SN38, Tu's team [59] designed a GSH-activated self-delivering nanomedicine, termed d-SNC NPs (Figure 4f). This disulfide-linked prodrug design takes advantage of the markedly higher intracellular GSH concentration in tumor cells (1–10 mM) compared with the extracellular environment (2–20 μM), thereby enabling GSH-triggered selective drug release. In this nanoparticle system, SN38 dimers were linked via disulfide bonds and co-loaded with Ce6, achieving an ultrahigh drug-loading capacity of approximately 85 wt%. In the GSH-rich tumor microenvironment, d-SNC NPs could specifically disassemble and release active SN38 and Ce6, thereby initiating synergistic chemotherapy and PDT, enhancing antitumor efficacy, and reducing systemic toxicity. DLS analysis showed that the hydrodynamic diameter of d-SNC NPs was approximately 154 nm (Figure 4g). Their fluorescence intensity increased with incubation time and approached the level of free Ce6 (Figure 4h). Under laser irradiation, d-SNC NPs exhibited the most pronounced inhibitory effect on 4T1 tumor growth (Figure 4i), with therapeutic efficacy clearly superior to that of PDT or chemotherapy alone, while showing no significant cytotoxicity to normal cells (Figure 4j). For chlorin-based PSs, Ce6-containing nanoplatforms remain a representative research direction because of their favorable photophysical properties and compatibility with different delivery systems [60,61]. Oxygen-generating and GSH-responsive nanosystems provide effective approaches to overcome tumor hypoxia and improve therapeutic selectivity [62]. Compared with single PDT, these microenvironment-responsive systems can produce stronger tumor inhibition through oxygen supplementation, chemotherapy, or redox-triggered drug release. Nevertheless, their therapeutic outcomes still depend on the heterogeneity of the tumor microenvironment, such as local H_2O_2 or GSH levels, and further pharmacokinetic and long-term safety evaluations are needed.

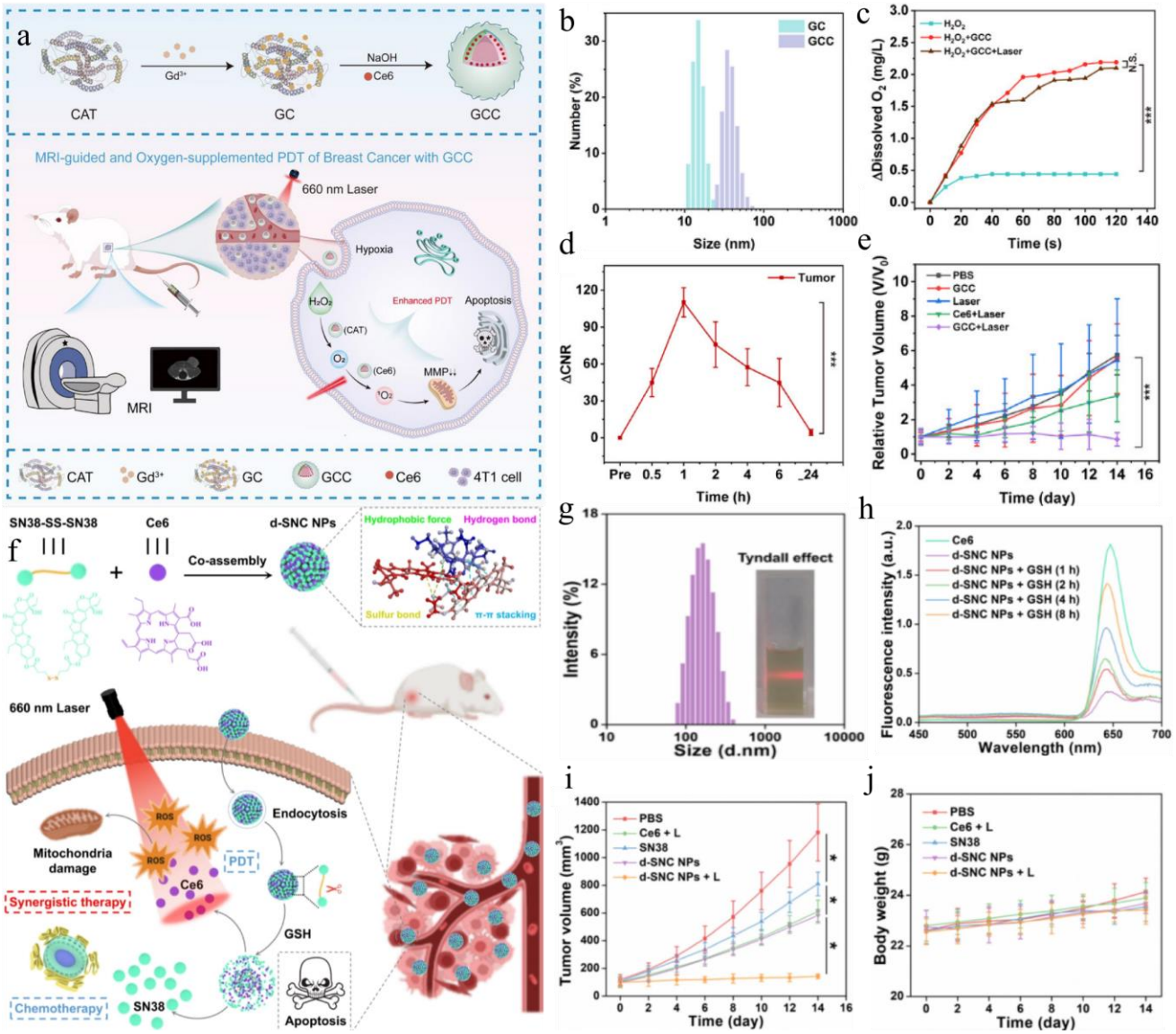

Figure 4. GCC and d-SNC NPs for photodynamic therapy. **(a)** Schematic diagram of GCC synthesis; **(b)** Hydrodynamic diameter distribution of GC and GCC; **(c)** Oxygen generation with and without laser illumination; **(d)** MRI signal intensity of tumors before and after intravenous injection of GCC; **(e)** Relative tumor volume changes in tumor-bearing mice after different treatments; **(f)** Schematic diagram of the co-assembly process of d-SNC nanoparticles and their chemo-photodynamic synergistic therapy mechanism; **(g)** Hydrodynamic diameter distribution of d-SNC; **(h)** Fluorescence spectra of Ce6, d-SNC nanoparticles and after incubation with GSH for different times; Tumor volume changes **(i)** and body weight changes **(j)** in tumor-bearing mice after different treatments.

2.3. Phthalocyanines

Phthalocyanine-based PSs exhibit long-wavelength absorption and high chemical stability, making them suitable for combined PDT/PTT therapy [63]. Wang's team [64] designed and constructed multifunctional nanoaggregates, termed PB/Z-S@B NAs (Figure 5a). Under 808 nm laser irradiation, the Prussian blue (PB) shell converts light into heat through the surface plasmon resonance effect, while the encapsulated ZnPc

generates singlet oxygen under 660 nm irradiation. These two therapeutic effects are spatially co-localized within the same nanoparticle, while their activation can be independently controlled in time by dual-wavelength irradiation. In addition, the PB shell enhances tumor vascular permeability through photothermal heating, thereby promoting the deep penetration of nanoparticles into tumors. The introduction of SAS biochemically inhibits GSH synthesis, reducing the resistance of tumor cells to oxidative damage. In this system, bovine serum albumin was used as a carrier to co-load the photosensitizer ZnPc and the GSH inhibitor sulfasalazine. A Prussian blue layer was then coated on the surface through in situ oxidative polymerization, forming a uniform core–shell nanostructure with a particle size of approximately 180 nm (Figure 5b). Five laser on/off cycling tests showed nearly consistent temperature changes without obvious performance attenuation (Figure 5c), indicating the excellent photothermal stability of the nanoaggregates. The absorbance of DPBF decreased with increasing irradiation time, demonstrating that PB/Z-S@B NAs could efficiently generate $^1O_2$ under 660 nm laser irradiation (Figure 5d). Under dual 660/808 nm laser irradiation, complete tumor eradication was achieved, with the tumor volume approaching zero after treatment (Figure 5e).

Although phthalocyanine-based PSs exhibit excellent performance, silicon phthalocyanines mainly operate through a type II mechanism and are prone to hydrophobic aggregation [65,66]. Moreover, conventional loading strategies often introduce inactive components, thereby reducing the effective photosensitizer content [67]. To address this issue, Su's team [68] designed axially substituted morpholine-containing silicon phthalocyanine derivatives and further cationized the nitrogen atom of the morpholine ring to obtain a cationic derivative, NP_2 (Figure 5f). The introduction of the cationic morpholine substituent alters the photophysical pathway of silicon phthalocyanine at the electronic level. As a strong electron-withdrawing group, this substituent lowers the excited-state reduction potential of the photosensitizer, making it more likely to accept electrons from surrounding substrates, such as NADPH or unsaturated lipids, and subsequently transfer these electrons to O_2 to generate superoxide radicals through a type I mechanism. Compared with the type II mechanism, which relies on energy transfer, this electron-transfer pathway is less sensitive to oxygen levels. Therefore, it can continuously generate ROS even under hypoxic conditions. The cationic substituent acts as a strong electron acceptor, effectively promoting charge separation and transfer. As a result, the spherical nanoparticles exhibit efficient type I PDT performance and can generate superoxide anion radicals (O_2^-) efficiently under both normoxic and hypoxic conditions (Figure 5g). NP_2 also shows strong fluorescence intensity and excellent photostability (Figure 5h). Under 660 nm laser irradiation, NP_2 effectively promoted the healing of Staphylococcus aureus-infected wounds, with an efficacy comparable to that of the streptomycin control group (Figure 5i). In addition, NP_2 exhibited favorable *in vivo* biosafety (Figure 5j), providing a solid foundation for its potential clinical application as an antibacterial phototherapeutic agent. For phthalocyanine-based PSs, the major advantage lies in their long-wavelength absorption and high photostability, which make them suitable for deep-tissue phototherapy and combined PDT/PTT [69]. Recent studies have shown that rational nanoassembly and axial modification can reduce aggregation, enhance ROS production, and even shift the photodynamic mechanism toward Type I pathways [70]. However, hydrophobic aggregation, limited aqueous dispersibility, and the introduction of inactive carrier components remain important issues [71]. Carrier-free or high-loading nanoplatforms may therefore be promising directions for improving the effective photosensitizer content and translational potential.

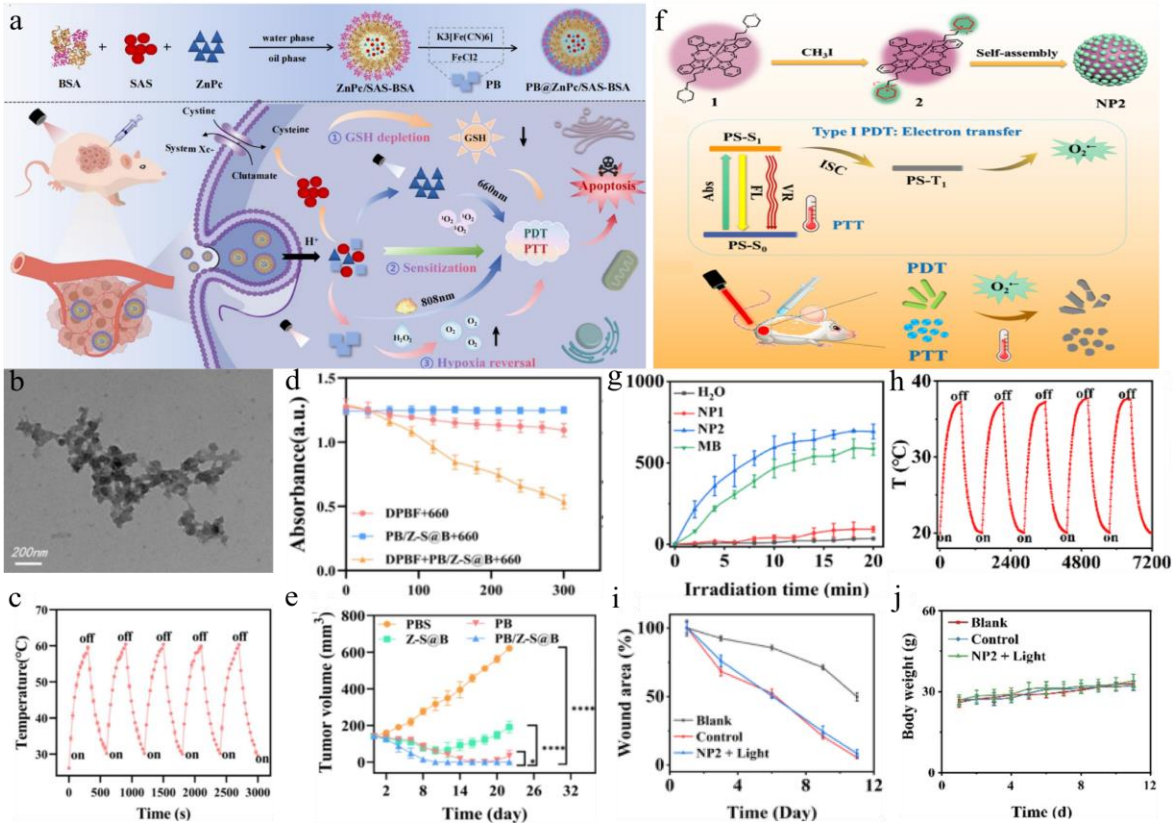

Figure 5. PB/Z-S@B NA and NP_2 for photodynamic therapy. **(a)** Synthesis route of PB/Z-S@B NA; **(b)** TEM image of PB/Z-S@B NA; **(c)** Photothermal cycling stability curve; **(d)** ROS detection curve of PB/Z-S@B NA under light irradiation; **(e)** Tumor growth curves of mice in different treatment groups; **(f)** Schematic diagram of nanomaterial preparation and tumor treatment; **(g)** O_2^- generation of NP_1, NP_2, and MB detected by DHE after irradiation; **(h)** Photothermal cycling stability curve; **(i)** Therapeutic effect on mice; **(j)** Changes in mice body weight over time.

2.4. Fused-ring quinones

Fused-ring quinone-based PSs are derived from natural products and possess efficient ROS-generating capability, enabling the induction of ICD [72]. Zhou's team [73] constructed a ferrocene-integrated Hyp self-assembled nanocomposite, termed PEG-PFc/Hyp (Figure 6a), by encapsulating Hyp within ferrocene-containing amphiphilic copolymer micelles. Ferrocene can catalyze Fenton reactions by reacting with H_2O_2 under acidic conditions to generate ·OH, while simultaneously consuming GSH and inhibiting GPX4 activity, thereby inducing ferroptosis. Under 595 nm light irradiation, Hyp produces $^1O_2$, directly killing tumor cells. These two types of ROS, ·OH and $^1O_2$, are generated concurrently within the same spatial region, leading to synergistically amplified oxidative stress. Moreover, O_2 produced during the Fenton reaction further alleviates tumor hypoxia and provides additional substrate for the type II photodynamic reaction of Hyp. Lipid peroxidation products induced by ferroptosis, together with damage-associated molecular patterns (DAMPs) generated by PDT, jointly activate antitumor immune responses, thereby linking local tumor destruction with systemic immune activation. Under 595 nm laser irradiation, Hyp generated abundant ROS. Meanwhile, ferrocene produced hydroxyl radicals (·OH) through a Fenton reaction, consumed GSH, and inhibited GPX4 activity, thereby inducing ferroptosis. The catalytically generated O_2 could further alleviate tumor hypoxia and amplify ROS production during

PDT. The synergistic effects of PDT, ferroptosis, and hypoxia relief markedly enhanced oxidative damage and induced ICD, leading to the release of damage-associated molecular patterns (DAMPs) and activation of antitumor immunity. PEG-PFc/Hyp nanocomposites showed a uniform particle size, with an average hydrodynamic diameter of approximately 122 nm (Figure 6b). Under 595 nm laser irradiation, GSH levels in 4T1 cells were depleted to approximately 20%, which was significantly lower than those in the free Hyp + PDT group and the non-irradiated groups (Figure 6c). The tumor inhibition rate reached 98.4%, with a marked reduction in tumor volume (Figure 6d), while good *in vivo* biosafety was also observed (Figure 6e).

To develop oxygen-independent type I PDT, which generates O_2^- and OH through electron transfer, as well as a long-wavelength two-photon PDT strategy, Zhang's team [74] designed a D–A–D-type type I aggregation-induced emission (AIE) photosensitizer, tBuT2AQ, using anthraquinone (AQ) as the central acceptor unit coupled with tert-butyl-modified triphenylamine (tBuTPA) (Figure 6f). The molecular basis of AIE lies in the twisted arrangement of the tBuTPA donor units around the AQ core. In the aggregated state, this configuration restricts intramolecular motion (RIM), thereby suppressing nonradiative transitions and enhancing fluorescence emission and photosensitization efficiency. In the D–A–D structure, AQ acts as a strong electron acceptor, while tBuTPA serves as the donor, enabling intramolecular charge transfer (ICT) from the donor to the acceptor. This charge-separated state favors the electron-transfer pathway, namely the type I mechanism, over the energy-transfer pathway associated with the type II mechanism. In addition, the planar structure of anthraquinone provides the molecule with a relatively large two-photon absorption cross-section, allowing it to reach the excited state through the simultaneous absorption of two photons under 940 nm excitation, thereby enabling photodynamic activation in deep tissues. AQ possesses strong electron affinity, high intersystem crossing efficiency, and redox cycling capability, which favor efficient OH generation. In addition, its planar structure endows the PS with excellent two-photon absorption properties, enabling deep-tissue penetration. By encapsulating tBuT2AQ with the acid-responsive charge-reversal polymer PCL-b-PAE, the resulting tBuT2AQ-PAE nanoparticles acquired a positively charged surface in the acidic tumor microenvironment, thereby enhancing cellular uptake and tumor accumulation. These nanoparticles exhibited a uniform size of 91.3 nm with a PDI of 0.20 (Figure 6g). Under 940 nm two-photon laser excitation, their ROS generation efficiency was higher than that of Ce6 (Figure 6h). Under simulated acidic tumor microenvironment conditions (pH 6.5), the cell viability decreased to approximately 10% (Figure 6i), demonstrating microenvironment-specific activation of PDT. Under 940 nm two-photon laser irradiation, tBuT2AQ-PAE NPs significantly inhibited the growth of PC3 prostate cancer tumors, with the relative tumor volume much smaller than that of the control group (Figure 6j). In contrast, treatment with laser irradiation alone or nanoparticles alone showed no obvious therapeutic effect, confirming the specific activation of PDT. For fused-ring quinone-based PSs, natural-product-derived structures such as hypericin and anthraquinone derivatives show strong ROS-generating ability and can be integrated with ferroptosis, hypoxia modulation, or two-photon excitation [75,76]. These studies suggest that fused-ring quinone PSs are not limited to conventional PDT but can also participate in cascade oxidative damage and immune activation. However, their clinical translation may still be influenced by poor water solubility, possible dark toxicity, and the need for carefully optimized nanocarriers. More systematic comparisons of phototoxicity, dark toxicity, metabolism, and immune effects are required.

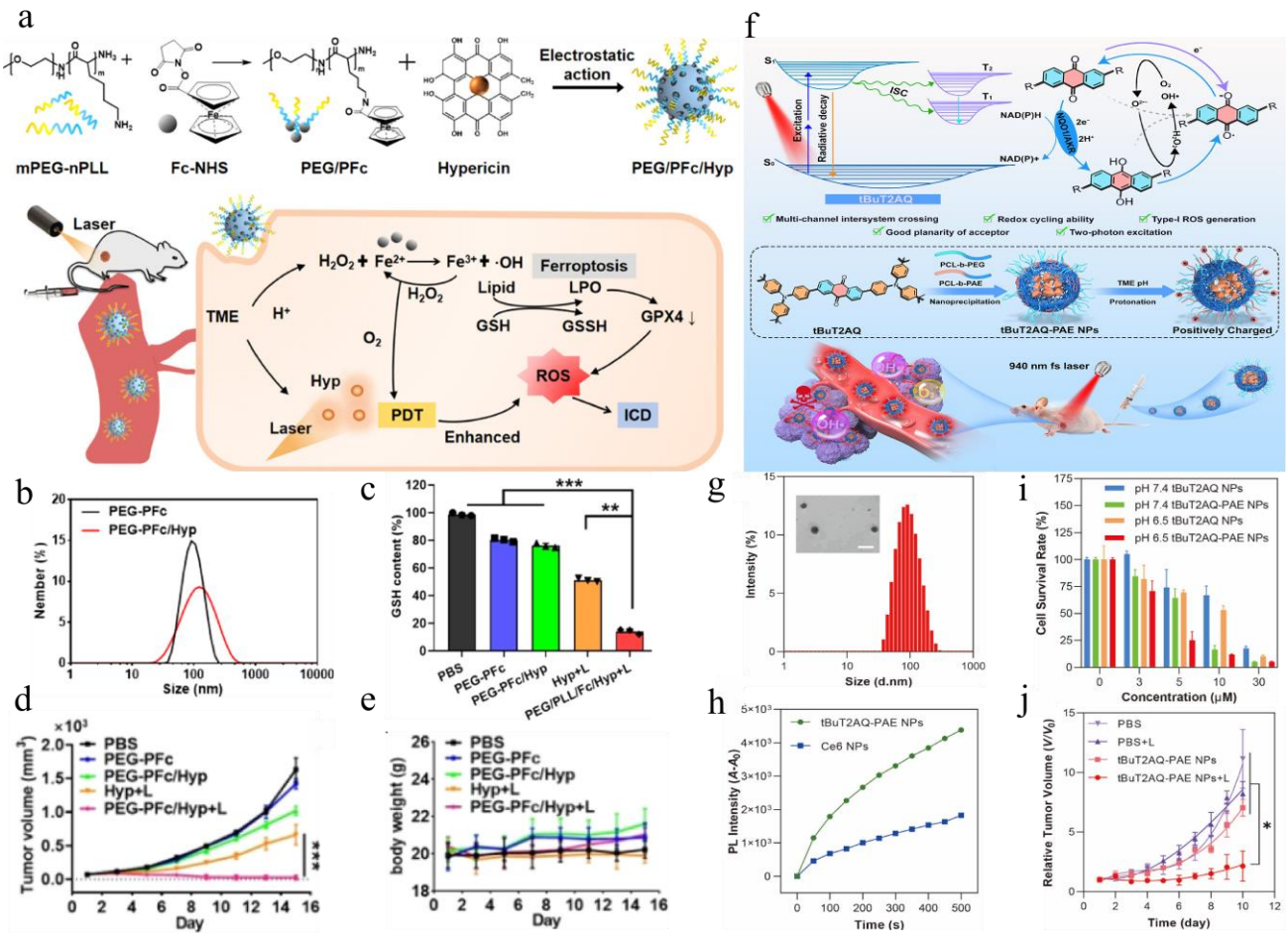

Figure 6. PEG-PFc/Hyp and tBuT2AQ-PAE for photodynamic therapy. **(a)** Schematic diagram of the preparation of PEG-PFc/Hyp and its anti-tumor therapy; **(b)** Hydrodynamic sizes of PEG-PFc/Hyp and PEG-PFc; **(c)** Intracellular GSH content in tumor cells after different treatments; Changes in tumor volume **(d)** and body weight **(e)** of mice over time after different treatments; **(f)** Schematic diagram of material design and its application in type I photodynamic tumor therapy; **(g)** Hydrodynamic size of tBuT2AQ-PAE nanoparticles in PBS; **(h)** Photoluminescence intensity of DCFH generated by tBuT2AQ-PAE NPs and Ce6; **(i)** Cell viability of PC3 cells treated with tBuT2AQ-PAE NPs and tBuT2AQ NPs at pH 6.5 or 7.4; **(j)** Changes in relative tumor volume of tumor-bearing mice receiving different treatments.

2.5. Phenothiazines

Phenothiazine-based PSs possess a butterfly-like molecular skeleton, and their type I radical-generation mechanism makes them particularly suitable for hypoxic tumors. Chen's team [77] proposed a molecular design strategy involving the grafting of flexible groups onto a rigid D–A conjugated backbone (Figure 7a). In EL-TPO2F, the rigid planar structure of the EDOT unit enhances molecular conjugation, thereby increasing the molar extinction coefficient and light-harvesting efficiency. Meanwhile, the introduction of long alkyl chains improves molecular flexibility and, through steric effects, helps prevent intermolecular π–π stacking and the formation of aggregates that are unfavorable for ROS generation. This "rigid–flexible" molecular design strategy balances enhanced light absorption with suppressed aggregation at the molecular level. As a result, the nanoparticles can maintain high light-harvesting

capability while preserving effective charge separation, thereby improving electron-transfer efficiency under the type I photodynamic mechanism. Using phenothiazine and triphenylamine as dual electron donors and tricyanofuran as the electron acceptor, they constructed four D–A-type PSs, namely TPSF, TPSSF, TPO2F, and EL-TPO2F, through different π-bridges, including thiophene, bithiophene, and EDOT. TPO2F NPs and EL-TPO2F NPs prepared by the nanoprecipitation method exhibited uniform spherical morphology, good dispersibility, and hydrodynamic diameters of 90–95 nm (Figure 7b). Among them, EL-TPO2F showed the strongest overall ROS-generating capability under 660 nm laser irradiation (Figure 7c). This was attributed to the synergistic effect of the rigid planar structure introduced by EDOT, which enhanced light absorption, and the long alkyl chains, which suppressed π–π stacking. Both nanoparticles significantly inhibited the growth of HepG2 liver cancer tumors under 660 nm laser irradiation, with the EL-TPO2F NPs + L group showing the best therapeutic efficacy (Figure 7d).

Compared with conventional apoptosis, programmed cell death pathways such as ferroptosis and pyroptosis can induce stronger inflammatory responses and promote the release of damage-associated molecular patterns (DAMPs), thereby more effectively stimulating antitumor immunity [78]. Chen's team [79] developed a PNBSe molecule (Figure 7e) by conjugating a selenium-substituted benzophenothiazine photosensitizer with pyrazolinone, enabling precise and long-lasting anchoring to the cell membrane. The pyrazolinone modification endows PNBSe with strong affinity for the phospholipid bilayer of the cell membrane, allowing it to localize on the cell membrane surface even before light irradiation. The key significance of this anchoring strategy is that short-lived photo-generated ROS do not need to diffuse through the cytoplasm. Instead, they can directly oxidize membrane lipids at the site of generation, rapidly disrupting membrane integrity and inducing cell necrosis. This mechanism is much faster than conventional PDT pathways that rely on endosome–lysosome trafficking. Moreover, necrosis-associated release of DAMPs, such as calreticulin (CRT) and high-mobility group box 1 (HMGB1), is more immunogenic. Upon light irradiation, PNBSe generated sufficient ROS at the cell membrane, inducing rapid membrane rupture and necrosis, followed by the release of intracellular contents and DAMPs, such as CRT and HMGB1. This process promoted dendritic cell maturation and activated T-cell-mediated adaptive immunity. Under 660 nm laser irradiation, PNBSe exhibited potent phototoxicity against various tumor cells (Figure 7f). By combining membrane anchoring with efficient ROS generation, it enabled precise and rapid induction of necrosis. In an orthotopic breast tumor model, the PNBSe-treated group achieved nearly complete tumor ablation, with therapeutic efficacy markedly superior to that of the PBS and PNBSe-alone groups (Figure 7g). For phenothiazine-based PSs, recent molecular engineering strategies demonstrate the value of Type I ROS generation under hypoxic conditions. The introduction of donor–acceptor structures, selenium substitution, or membrane-anchoring groups can improve ROS generation, subcellular localization, and ICD [80,81]. Compared with conventional Type II PSs, these systems may be more suitable for hypoxic solid tumors. However, excessive membrane damage or necrosis-related inflammation should be carefully evaluated, and the relationship between local tumor destruction and systemic immune activation requires further investigation.

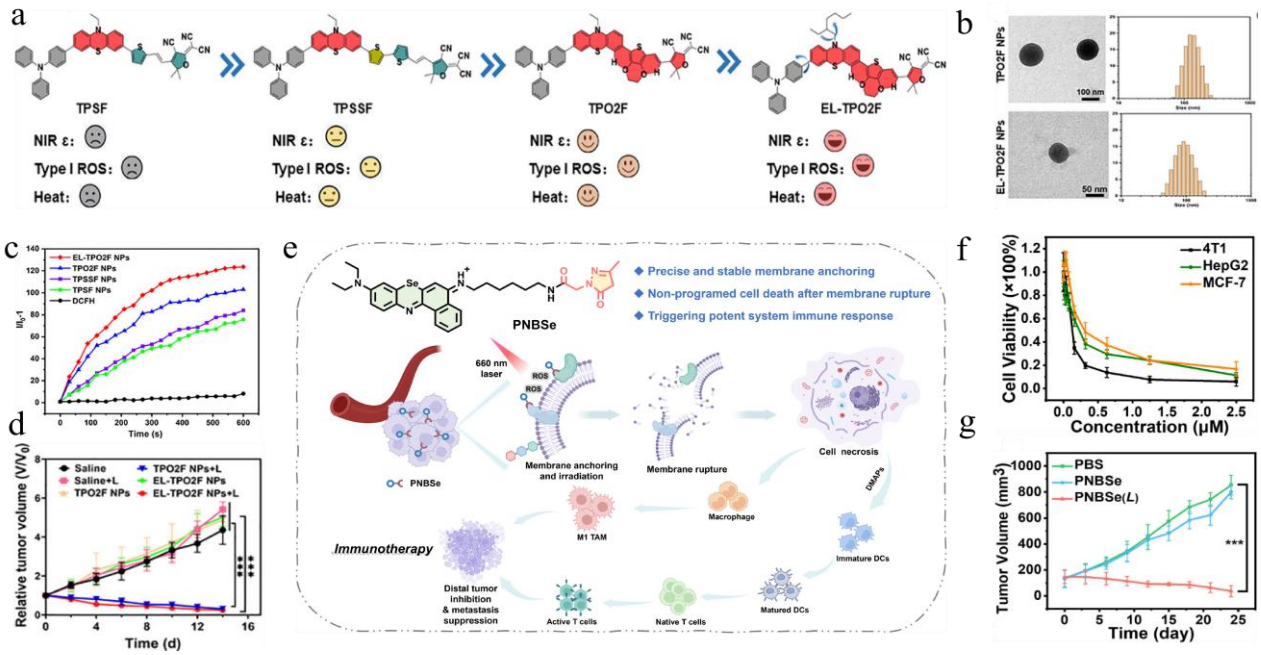

Figure 7. TPO2F/EL-TPO2F and PNBSe for photodynamic therapy. **(a)** Design and performance optimization of phenothiazine-based Type I PSs; **(b)** Transmission electron microscopy images and dynamic light scattering curves of TPO2F NPs and EL-TPO2F NPs; **(c)** ROS performance testing of PSs; **(d)** Relative tumor volume changes in mice during different treatment processes; **(e)** Mechanism of PNBSe activating anti-tumor immunity through cell necrosis induced by cell membrane rupture; **(f)** Phototoxicity of PNBSe in different tumor cells; **(g)** Changes in mouse tumor volume over time after different treatments.

2.6. BODIPY derivatives

BODIPY-based PSs, with boron-dipyrromethene as the core structure, exhibit high photostability and high fluorescence quantum yields. Through structural modification, their absorption can be extended into the NIR-II window [82]. Zhang's team [83] introduced 1,4-dimethyl-1,2,3,4-tetrahydroquinoxaline (NN) units at the 3,5-positions of aza-BODIPY and combined them with a strongly electron-withdrawing CF_3 group to construct a D–A–A′-type molecule, CF_3-NN (Figure 8a). The structural basis for the NIR-II absorption of CF_3-NN lies in the three-step charge-transfer process within the D–A–A′ framework: electron donation from the NN donor units to the aza-BODIPY core, the further electron-withdrawing effect of the CF_3 group, and the intrinsic electron-deficient nature of the aza-BODIPY core itself. Together, these effects markedly narrow the HOMO–LUMO energy gap. This narrowed energy gap red-shifts the absorption wavelength to 990 nm, extending it into the NIR-II window. Within this wavelength range, photon scattering is reduced, allowing light to penetrate tissues to a depth of several centimeters. CF_3-NN showed an absorption peak at 944 nm in dichloromethane, while in DMSO it exhibited red-shifted absorption/emission peaks at 990/1240 nm, located within the NIR-II window. CF_3-NN NPs displayed a uniform spherical morphology in aqueous solution, with a hydrodynamic diameter of approximately 150 nm, a narrow size distribution, and good dispersibility (Figure 8b). Five laser on/off cycles showed nearly consistent temperature changes without obvious performance attenuation (Figure 8c), indicating excellent photothermal stability. Under 915 nm laser irradiation, CF_3-NN NPs rapidly and completely ablated 4T1 breast tumors (Figure 8d). Tumor volume decreased by 87% on day 2 after treatment,

completely disappeared by day 6, and showed no recurrence within 18 days. Good *in vivo* biosafety was also observed (Figure 8e).

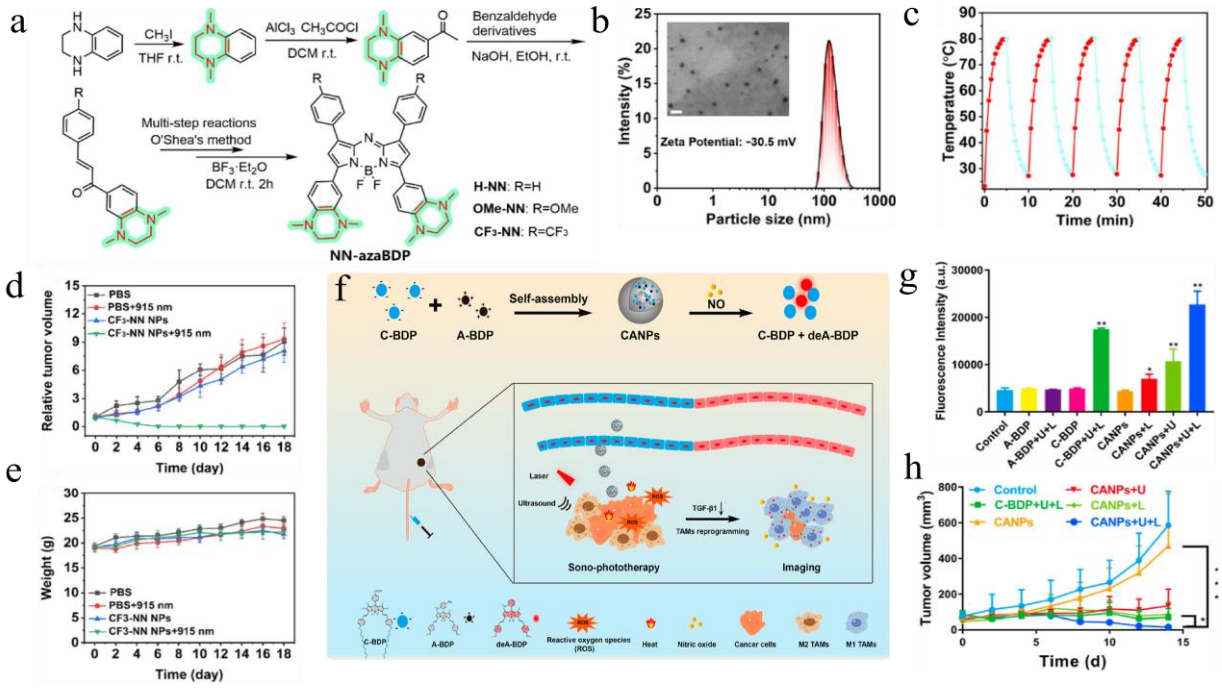

Figure 8. NN-azaBDPs and CANPs for photodynamic therapy. **(a)** Synthetic route of NN-azaBDPs; **(b)** TEM images and DLS characteristics of CF_3-NN nanoparticles; **(c)** Cyclic stability of CF_3-NN nanoparticles under NIR light irradiation; Tumor volume **(d)** and changes in mouse body weight **(e)** after different treatments; **(f)** Schematic diagram of self-assembled CANPs preparation and therapeutic diagnostic mechanism; **(g)** Quantitative flow cytometry analysis of 4T1 cells stained with DCFH-DA; **(h)** Tumor growth curves of tumor-bearing mice after different treatments.

Li's team [84] designed an amino-BODIPY probe, A-BDP, as a tumor-associated macrophage (TAM)-targeted fluorescent probe for monitoring nitric oxide (NO) produced by M1 TAMs. However, this probe suffers from poor water solubility and a tendency to aggregate. To overcome these limitations, the team constructed a carrier-free nanotheranostic system, termed CANPs (Figure 8f), through the self-assembly of negatively charged amphiphilic iodine-substituted BODIPY, C-BDP, which possesses both sonosensitizing and photosensitizing properties, and positively charged A-BDP via electrostatic interactions, π–π stacking, and hydrogen bonding. Under combined ultrasound and laser irradiation, CANPs enabled C-BDP-mediated synergistic sonodynamic/PDT, while A-BDP allowed real-time fluorescence monitoring of TAM reprogramming through NO release. The study further revealed that transforming growth factor-β (TGF-β) is a key factor in sono-phototherapy-induced remodeling of the tumor microenvironment. Under combined ultrasound and laser irradiation, CANPs efficiently induced intracellular ROS generation in 4T1 cells (Figure 8g), producing significantly higher ROS levels than those achieved with single irradiation or free C-BDP. CANPs also exhibited the strongest antitumor efficacy, resulting in the smallest tumor volume (Figure 8h). For BODIPY-based PSs, structural modification enables absorption/emission extension into the near-infrared or NIR-II region, while self-assembled nanotheranostic systems further integrate imaging, PDT, PTT, or sonodynamic therapy [85,86]. These features make BODIPY derivatives attractive for image-guided and multimodal

tumor therapy. Nevertheless, many BODIPY systems still require improved water solubility, reduced dark toxicity, and clearer *in vivo* metabolic profiles. Future work should focus not only on red-shifting absorption and enhancing ROS generation but also on simplifying nanoplatform design and strengthening biosafety evaluation.

3. Conclusion

The diverse chemical structures of organic PSs endow them with distinct photophysical properties and ROS-generation mechanisms (Table 1). Among them, porphyrin- and chlorin-based PSs are relatively well established in clinical applications, whereas phthalocyanine- and BODIPY-based PSs show greater potential in near-infrared absorption and multimodal therapy. Through nanostructuring strategies such as self-assembly, biomimetic mineralization, and cell membrane anchoring, the water solubility, tumor accumulation, and cellular uptake efficiency of PSs have been significantly improved. These strategies also help overcome the aggregation-caused quenching and nonspecific toxicity associated with conventional PSs.

Table 1. Representative organic photosensitizer-based nanoplatforms for tumor PDT.

Photosensitizer type	Material	ROS generation mechanism	Absorption wavelength range (nm)	Oxygen dependence	Photostability	Nanodelivery strategy	Reference
Porphyrin	GA-IS	Type II	600–650	High	Good	PROTAC technology and Golgi-targeted nanoassembly	[51]
	DA-Cys-PD	Type II	550–650	High	Good	Cell membrane anchored click chemistry-mediated *in situ*assembly	[56]
Chlorin	Gd@CATCE6 (GCC)	Type II	650–680	High	Moderate	Catalase-templated biomimetic mineralized nanoprobe	[58]
	d-SNC NPs	Type II	650–680	High	Good	GSH-responsive prodrug self-delivery nanoparticles	[59]
Phthalocyanine	PB/Z-S@BNAs	Type I	680–700	Low	Excellent	BSA encapsulation and Prussian blue surface functionalization	[64]
Fused-ring quinone	PEG-Pfc/hypericin (Hyp)	Type II	550–600	High	Moderate	Ferrocene-integrated self-assembled nanocomposite	[73]
	tBuT2AQ-PAE NPs	Type I	450–500	Low	Good	PCL-b-PAE acid-responsive charge-reversal polymer	[74]
Phenothiazine	TPO2F NPs and EL-TPO2F NPs	Type I	600–670	Low	Moderate	Nanoparticles prepared by the nanoprecipitation method	[77]
BODIPY	PNBSs	Type II	640–660	High	Good	Cell membrane anchoring molecule	[79]
	CF_3-NN	Type I	944–990	Low	Excellent	Self-assembled nanoparticles	[83]
	CANPs	Type II	660–680	High	Good	Carrier-free electrostatic/π–π self-assembled nanotheranostic system	[84]

Despite the continued advancement of these innovative strategies, AIE materials, NIR-II (1000–1700 nm) PSs, and two-photon excitation PDT have emerged as three highly active and interconnected frontier directions in tumor PDT. AIE materials fundamentally overcome the aggregation-caused quenching of conventional PSs induced by π–π stacking in physiological environments through the restriction of intramolecular motion (RIM) mechanism, allowing PSs to retain efficient ROS generation after nanoassembly or targeted binding [87]. Based on this principle, recently developed "turn-on" AIE PSs can precisely activate ROS generation in response to tumor microenvironment-specific stimuli, such as enzyme responsiveness, pH responsiveness, or aggregation induced by solubility changes [88]. In contrast, "turn-off" designs enable rapid inactivation after treatment through self-degradation or ROS-responsive cleavage of chemical bonds, thereby effectively reducing persistent skin phototoxicity caused by residual conventional PSs [89]. Meanwhile, PSs operating in the NIR-II window take advantage of the low photon scattering coefficient in this spectral region, enabling tissue penetration depths of several centimeters and making phototherapy for deep-seated tumors possible [90]. Their molecular design mainly relies on the synergistic narrowing of the bandgap through donor–acceptor (D–A) engineering and fluorination strategies, together with the incorporation of heavy-atom effects to promote intersystem crossing efficiency. Two-photon excitation technology enables deep photodynamic activation with high spatial precision at the submicron level through the simultaneous absorption of two near-infrared photons. Since the excitation probability is proportional to the square of the light intensity, this approach inherently possesses three-dimensional spatial selectivity. Notably, these three directions are not developing in isolation. AIE characteristics endow NIR-II PSs with enhanced fluorescence and photosensitization efficiency in the aggregated state, while two-photon excitation is highly compatible at the molecular level with the extended π-conjugated systems and D–A–D architectures of AIE molecules [91]. However, despite their rapid development, these frontier strategies still face major challenges. The narrow bandgap required for NIR-II absorption is often accompanied by enhanced photothermal competition, requiring a delicate balance between ROS quantum yield and photothermal conversion efficiency. Two-photon excitation depends on expensive femtosecond lasers, and its clinical translation is limited by equipment cost and operational complexity. The selectivity and response kinetics of "turn-on/turn-off" AIE PSs in complex *in vivo* environments also require systematic validation. In addition, most current studies remain limited to subcutaneous xenograft models. Their performance in orthotopic and immunocompetent models, which more closely resemble real clinical settings, as well as head-to-head comparisons with clinically approved PSs, remain largely unexplored but critically important evaluation steps.

Current research has evolved from single-modality PDT toward multimodal synergistic therapy combined with ferroptosis, immunotherapy, chemotherapy, and photothermal therapy. These combined strategies can amplify tumor cell death, activate systemic antitumor immune responses, and overcome the limitations imposed by the hypoxic tumor microenvironment. In addition, tumor microenvironment regulation, such as oxygen supply, GSH depletion, and pH responsiveness, together with multimodal imaging guidance, including MRI and fluorescence imaging, further improves the precision and controllability of PDT. Despite these advances, several inherent limitations remain. The oxygen dependence of conventional type II PSs remains a fundamental obstacle in hypoxic solid tumors. Although type I PSs provide an alternative strategy, their overall ROS generation efficiency is often relatively low, and systematic comparative evaluations remain insufficient. The tissue penetration depth

of visible light and even NIR-I light is still limited, while NIR-II and two-photon strategies, although promising, remain at an early stage of clinical translation. Poor tumor specificity may lead to off-target accumulation and prolonged skin photosensitivity, which represents a major concern affecting patients' quality of life. Moreover, the heterogeneity of the tumor microenvironment further complicates the universal applicability of any single photosensitizer design, and the lack of standardized preclinical benchmarks hinders objective evaluation of therapeutic progress.

Future studies should focus on developing highly efficient oxygen-independent type I PSs to overcome the restrictions of the hypoxic microenvironment in solid tumors on conventional PDT. Meanwhile, long-wavelength technologies, such as NIR-II window absorption and two-photon excitation, should be further expanded to enable precise photodiagnosis and phototherapy of deep-seated tumors. Smart responsive nanosystems, including carriers that can be specifically activated by GSH, pH, enzymes, or ROS in the tumor microenvironment, will become an important direction for improving therapeutic specificity and reducing nonspecific toxicity. In terms of therapeutic strategies, the in-depth combination of PDT with immunotherapies such as immune checkpoint inhibitors and CAR-T therapy deserves further exploration, which may promote the transition of PDT from a local treatment modality to systemic immune activation. From a translational perspective, it is urgently necessary to strengthen pharmacokinetic, toxicological, and therapeutic efficacy studies of novel PSs in large-animal models. Standardized comparisons with clinically approved PSs should also be routinely conducted to enable objective performance evaluation. These efforts will accelerate the clinical translation of PSs with high photodynamic performance and favorable biosafety, ultimately facilitating their clinical application.

Declaration of generative AI and AI-assisted technologies

The authors did not use generative AI or AI-assisted technologies in the writing of this manuscript.

Acknowledgments

This work was funded by the National Natural Science Foundation of China (22171163), the 111 Project of China (D20015) and the Yichang Natural Science Research Program (A23-2-025).

Authors' contribution

Investigation, Q.J., Y.H., W.W., H.L., S.X., W.Z. and P.G.; writing—original draft preparation, Q.J. and Y.H.; writing—review and editing, S.X., W.Z. and P.G.; project administration, P.G.; funding acquisition, P.G. All authors have read and agreed to the published version of the manuscript.

Conflicts of interest

The authors declare no conflict of interest.

References

[1] Cheng H, Huang L, Huang J, Feng J, Huang K, *et al*. Cholesterol reprograms oxysterol metabolism via the LOX1/CH25H/CYP7B1 signaling axis to drive multidrug resistance in colorectal cancer. *Hum. Mutat.* 2026, 2026(1):3675889–3675889.

[2] Liu H, Zhang J, Rao Y, Jin S, Zhang C, *et al.* Intratumoral microbiota: an emerging force in diagnosing and treating hepatocellular carcinoma. *Med. Oncol.* 2024, 41(12):300.
[3] Wang W, Huang Y, Li Y, Geng P, Lan H, *et al.* Multifunctional metal–organic frameworks and their heterojunction materials for cancer theranostics. *Biomater. Sci.* 2025, 13:4081.
[4] Xu D, Hou C, Chang J, Yang S, Yang Z, *et al.* The effect of chloroquine on cervical cancer via the PI3K/AKT/MDM2 pathway. *Discover Oncol.* 2025, 16(1):1179.
[5] Wang W, Li Y, Li Y, Huang Y, Geng P, *et al.* Titanium-protoporphyrin IX coordinated nanoparticles for tumor photoZdynamic and sonodynamic combination therapy. *Biofunct. Mater*. 2025, 2:0009.
[6] Wang W, Zhang Y, Li Y, Huang Y, Xiao S, *et al.* Preparation of cuttlefish ink-porphyrin nanoconjugates and its application in photodynamic-photothermal synergistic treatment of tumor cells. *Nano Med. Mater.* 2024, 4(1):1895.
[7] Hou W, Shen L, Zhu Y, Wang X, Du X, *et al.* Fullerene derivatives for tumor treatment: mechanisms and application. *Int. J. Nanomed.* 2024, 19:9771–9797.
[8] Li Y, Wang W, Zhang Y, Xiao S, Lan H, *et al*. Design and synthesis of nanoscale Zr-porphyrin IX framework for synergistic photodynamic and sonodynamic therapy of tumors. *Acta Chim. Sin.* 2024, 82:448.
[9] Liang J, Lai X, Mei Y, Liu X, Wen S, *et al.* Oxygenation: nanotechnological strategies for conquering tumor hypoxia in photodynamic therapy. *Int. J. Nanomed.* 2026, 21:569340.
[10] Yang M, Yang T, Mao C. Enhancement of photodynamic cancer therapy by physical and chemical factors. *Angew. Chem. Int. Ed*. 2019, 58(40):14066–14080.
[11] Wang X, Wu J, Wu N. Inorganic particle-emulsion complex system as a vaccine adjuvant. *Chin. J. Biotechnol*. 2026, 46(5):26–39.
[12] Huang Y, Wang W, Li Y, Zhang Y, Geng P, *et al.* Research progress of multi-source photosensitizers in tumor treatment. *Chin. J. Biomed. Eng*. 2026, 45(2):243–251.
[13] Wang J, Zhang B. Bovine serum albumin as a versatile platform for cancer imaging and therapy. *Curr. Med. Chem*. 2018, 25(25):2938–2953.
[14] Huang Y, Jin Q, Wang W, Geng P, Xiang G, *et al*. Advanced strategies in nanosonosensitizer engineering for superior sonodynamic therapeutics. *Coordin. Chem. Rev*. 2026, 558:217800.
[15] Yang Y, Yang T, Chen F, Zhang C, Yin B, *et al.* Degradable magnetic nanoplatform with hydroxide ions triggered photoacoustic, mr imaging, and photothermal conversion for precise cancer theranostic. *Nano Letters*. 2022, 22(8):3228–3235.
[16] Liang C, Lu Y, Yin X. Research advances in nano-photodynamic therapy for treatment of cutaneous melanoma. *J. Acad. Mil. Med. Sci*. 2024, 45(10):1096–1102.
[17] Shao Y, Shen R, Wang S, Li S, Zhang P, *et al.* Component engineering in covalent organic frameworks for tailored photocatalysis. *Acta Phys.-Chim. Sin*. 2025, 41(12):7–54.
[18] Zhang J, Pan Y, He C, Wang Y, Miao X, *et al.* Progress of type i organic photosensitizers for photodynamic Therapy. *Chin. Laser* 2024, 51(15):98–117.
[19] Zhang T, Shi M, Ji X. Li T, Tang L, *et al*. Phase 0 clinical trials facilitate iteration of a new paradigm for original drug development in China. *Chin. Med. Biotechnol.* 2024, 19(3):193–196.
[20] Liao Y, Wang R, Wang S, Xie Y, Chen H, *et al*. Highly efficient multifunctional organic photosensitizer with aggregation-induced emission for *in vivo* bioimaging and photodynamic therapy. *ACS Applied Materials & Interfaces*. 2021, 13(46):54783–54793.

[21] Gu R, Zhang T, Si W, Dong X. Advances in research on nanosystem of tumor phototherapy combined with gas therapy. *Adv. Pharm*. 2021, 45(4):263–272.
[22] Nguyen V, Nguyen M, Pham T, Vu A, Nguyen T. Recent advances in near-infrared organic photosensitizers for photodynamic cancer therapy. *Biomater. Sci*. 2025, 13(5):1179–1188.
[23] Orlandi V, Martegani E, Trivellin N, Bolognese F, Caruso E. Photo-inactivation of staphylococcus aureus by diaryl-porphyrins. *Antibiotics* 2023, 12(2):228.
[24] Luo R, Xu H, Lin Q, Chi J, Ou J, *et al.* Emerging trends in dissolving-microneedle technology for antimicrobial skin-infection therapies. *Pharmaceutics* 2024, 16(9):1188.
[25] Yang Q, Sun X, Wang H, Chen T, Wang Z. Multi-modular metabolic engineering of heme synthesis in Corynebacterium glutamicum. *Synth. Syst. Biotechnol*. 2024, 9(2):285–293.
[26] Huang Y, Jin Q, Wang W, Zhang Y, Geng P, *et al.* Nanoengineering of porphyrin-based biomaterials for innovative cancer therapy. *Chem. Rec.* 2026, 26(5):e202500306.
[27] De L, Romeo A, Scolaro L, Ricciardi G, Rosa A. Sitting-atop metallo-porphyrin complexes: experimental and theoretical investigations on such elusive species. *Inorg. Chem*. 2009, 48(17):8493–8507.
[28] Howley R, Chandratre S, Bin C. 5-Aminolevulinic acid as a theranostic agent for tumor fluorescence imaging and photodynamic therapy. *Bioengineering* 2023, 10(4):496.
[29] Liang L, Wang W, Li M, Xu Y, Lu Z, *et al.* Cancer photodynamic therapy enabled by water-soluble chlorophyll protein. *ACS Appl. Mater. Interfaces* 2025, 17(11):16668–16680.
[30] Huggett MT, Jermyn M, Gillams A, Illing R, Mosse S, *et al.* Phase I/II study of verteporfin photodynamic therapy in locally advanced pancreatic cancer. *Br. J. Cancer* 2014, 110(7):1698–1704.
[31] Yang H, Liu R, Xu Y, Qian L, Dai Z. Photosensitizer nanoparticles boost photodynamic therapy for pancreatic cancer treatment. *Nano-Micro Lett.* 2021, 13(1):35.
[32] Sanders H, Price C, Barreto A, Rho S, Sullivan T, *et al*. Implanted miniature light devices for phototherapeutics. *Adv. Ther.* 2026, 9(1):e00492.
[33] Miretti M, Clementi R, Tempesti T, Baumgartner M. Photodynamic inactivation of multiresistant bacteria (KPC) using zinc(II)phthalocyanines. *Bioorg. Med. Chem. Lett*. 2017, 27(18):4341–4344.
[34] Nizovtsev AS. Optical spectrum of tetrafluorosubstituted zinc phthalocyanine. *J. Struct. Chem*. 2023, 64:1228–1236.
[35] Mitra R, Hartman, MCT. Silicon phthalocyanines: synthesis and resurgent applications. *Org. Biomol. Chem*. 2021, 19:1168–1190.
[36] Schmidt J, Kuzyniak W, Berkholz J, Steinemann G, Ogbodu R, *et al*. Novel zinc-and silicon-phthalocyanines as photosensitizers for photodynamic therapy of cholangiocarcinoma. *Int. J. Mol. Med*. 2018, 42(1):534–546.
[37] Mavridi-Printezi A, Guernelli M, Menichetti A, Montalti M. Bio-applications of multifunctional melanin nanoparticles: from nanomedicine to nanocosmetics. *Nanomaterials* 2020, 10(11):2276.
[38] Nash G, Luo T, Lan G, Ni K, Kaufmann M, *et al.* Nanoscale metal-organic layer isolates phthalocyanines for efficient mitochondria-targeted photodynamic therapy. *J. Am. Chem. Soc*. 2021, 143(5):2194–2199.
[39] Mohamed F, Anhlan D, Schofbanker M, Schreiber A, Classen N, *et al*. Hypericum perforatum and its ingredients hypericin and pseudohypericin demonstrate an antiviral activity against SARS-CoV-2. *Pharmaceuticals* 2022, 15(5):530.

[40] Abegg V, Panajatovic M, Mancuso R, Allard J, Duthaler U, *et al*. Mechanisms of hepatocellular toxicity associated with the components of St. John's Wort extract hypericin and hyperforin in HepG2 and HepaRG cells. *Toxicol. Lett*. 2024, 393:1–13.

[41] Khatoon N, Afthab J, Zhang Z, Chu M, Huang Y, *et al*. Hypocrellin A-cisplatin-intercalated hectorite nano formulation for chemo-photodynamic tumor-targeted synergistic therapy. *J. Mater. Sci*. 2024, 59:2087–2103.

[42] Lan J, Chen S, Chen Z, Luo D, Yu C, *et al*. Chemo-photodynamic antitumour therapy based on ER-doped upconversion nanoparticles coated with hypocrellin b and MnO_2. *Biomater. Adv*. 2024, 161:213891.

[43] Nadhan R, Patra D, Krishnan N, Rajan A, Gopala S, *et al*. Perspectives on mechanistic implications of ROS inducers for targeting viral infections. *Eur. J. Pharmacol*. 2021, 890:173621.

[44] Venkatesan K, Stayanarayana V, Sivakumar A, Ramamurthy C, Thirunavukkarusu C. Synthesis, spectral characterization and antitumor activity of phenothiazine derivatives. *J. Heterocycl. Chem*. 2020, 57(7):2722–2728.

[45] Ryabova A, Romanishkin I, Markova I, Pominova D. Simultaneous application of methylene blue and chlorin e6 photosensitizers: investigation on a cell culture. *Sovrem. Tekhnol. Med*. 2025, 17(1):58–68.

[46] Wu Y, Chen Y, Yao S, Li S, Yuan H, *et al*. Manipulating the subcellular localization and anticancer effects of benzophenothiaziniums by minor alterations of n-alkylation. *Molecules* 2023, 28(4):1714.

[47] Gutsche C, Ortwerth M, Grafe S, Flanagan K, Senge M, *et al*. Nucleophilic aromatic substitution on pentafluorophenyl-substituted dipyrranes and tetrapyrroles as a route to multifunctionalized chromophores for potential application in photodynamic therapy. *Chem. Eur. J*. 2016, 22(39):13953–13964.

[48] Deng L, Chen Z, Jiang L, Jing Q, Wang S, *et al*. Treatment of diabetic infection wounds using novel fluoroborane dipyrrole-coated transparent patch. *Bioorg. Chem*. 2025, 163:108678.

[49] Guseva G, Antina E, Berezin M, Smirnova A, Pavelyev R, *et al*. Design, spectral characteristics, photostability, and possibilities for practical application of BODIPY FL-Labeled thioterpenoid. *Bioengineering* 2022, 9(5):210.

[50] Bettini S, Valli L, Giancane G. Applications of photoinduced phenomena in supramolecularly arranged phthalocyanine derivatives: a perspective. *Molecules* 2020, 25(16):3742.

[51] Zheng R, Li Q, Zhang S, Zhou H, Chen G, *et al.* Golgi apparatus-targeting immunostimulant for synergistic activation of antitumor immunity via pyroptosis induction and PD-L1 degradation. *Adv. Healthc. Mater*. 2026, 0:e04895.

[52] Fernandez-Fernandez A, Manchanda R, McGoron AJ. Theranostic applications of nanomaterials in cancer: drug delivery, image-guided therapy, and multifunctional platforms. *Appl. Biochem. Biotechnol*. 2011, 165(7–8):1628–1651.

[53] Kim K. Hybrid Systems of. gels and nanoparticles for cancer therapy: advances in multifunctional therapeutic platforms. *Gels* 2025, 11(3):170.

[54] Zhou Z, Zhang S, Xue N. Research progress of cancer cell membrane coated nanoparticles for the diagnosis and therapy of breast cancer. *Front. Oncol*. 2023, 13:1270407.

[55] Ratay M, Bellotti E, Gottardi R, Little S. Modern therapeutic approaches for noninfectious ocular diseases involving inflammation. *Adv. Healthc. Mater*. 2017, 6(23):1700733.

[56] Ma Y, Liu X, Jiang Q, Xu H, Liang G, *et al*. Cell membrane-anchored click reaction enhances porphyrin uptake for highly efficient photodynamic therapy of breast tumors. *J. Am. Chem. Soc*. 2025, 147(45):41657–41667.

[57] Satrialdi, Takano Y, Hirata E, Ushijima N, Harashima H, *et al*. An effective in vivo mitochondria-targeting nanocarrier combined with a π-extended porphyrin-type photosensitizer. *Nanoscale Adv*. 2021, 3:5919–5927.

[58] Gu W, Liu D, Wu Y, Yang W, Yun Y, *et al*. Biomimetic catalase-templated nanoprobes for MRI-Guided oxygen-supplemented photodynamic therapy in breast cancer. *Adv. Healthc*. Mater. 2026, 15(19):e02430.

[59] Tu L, Huang R, Yin Q, Zhuo X, Zhu Y, *et al*. Glutathione-activated prodrug-based self-delivering nanomedicines for tumoricidal chemo-photodynamic synergistic therapy. *J. Colloid Interface Sci*. 2026, 707:139682.

[60] Huang X, Chen T, Mu N, Lam H, Sun C, *et al*. Supramolecular micelles as multifunctional theranostic agents for synergistic photodynamic therapy and hypoxia-activated chemotherapy. *Acta Biomater*. 2021, 131:483–492.

[61] Kim S, Cho E, Bae S, Kim S, Park D. The effect of a newly developed mini-light-emitting diode catheter for interstitial photodynamic therapy in pancreatic cancer xenografts. *J. Transl. Med*. 2021, 19:248.

[62] Wang L, Sun Y, Sun Y, Zhang C, Wang G, *et al.* GSH-Activated Cu-TCPP(zn)/Ti3C2Tx nanozymes for fluorescence imaging-guided synergistic photodynamic/chemodynamic therapy of oral squamous cell carcinoma. *ACS Appl. Mater. Interfaces* 2026, 18(9):13649–13669.

[63] Wang W, Xu H, Chen Z, Fu S, Wang C, *et al*. Modulation of phthalocyanine assembly morphology for photodynamic therapy. *Chem. Commun*. 2025, 61(99):19596–19607.

[64] Wang Q, Wu F, Qiu X, Yu H, Lu M, *et al*. Zinc phthalocyanine and sulfasalazine coloaded nanoaggregates with Prussian blue functionalization for sensitizing tumor photothermal/ photodynamic therapy. *J. Colloid Interface Sci*. 2025, 685:509–521.

[65] Schmidt J, Kuzyniak W, Berkholz J, Steinemann G, Ogbodu R, *et al*. Novel zinc- and silicon-phthalocyanines as photosensitizers for photodynamic therapy of cholangiocarcinoma. *Int. J. Mol. Med*. 2018, 42(1):534–546.

[66] Sahin S, Agar E. A3B type unsymmetrical and amphiphilic phthalocyanines: synthesis, characterization, thermal stability and aggregation studies. *Spectrochim. Acta A Mol. Biomol. Spectrosc*. 2020, 227:117694.

[67] Roberto M, La Cava F, Arena F, Cordaro A, Stummo F, *et al*. Peptide-guided photodynamic therapy via integrin αvβ6 in pancreatic cancer. *Int. J. Mol. Sci*. 2026, 27(4):1838.

[68] Su W, Luo X, Li P, Zhang Y, Lin C, *et al*. Phthalocyanine self-assembled nanoparticles for type I photodynamic antibacterial therapy. *Chin. Chem. Lett*. 2024, 35(12):109522.

[69] Grundke C, Silva R, Kitzmann W, Heinze K, Oliveira K, *et al*. Photochemical α-Aminonitrile synthesis using Zn-phthalocyanines as near-infrared photocatalysts. *J. Org. Chem*. 2022, 87(9):5630–5642.

[70] He L, Ma D. Self-assembled phthalocyanine-based nano-photosensitizers in photodynamic therapy for hypoxic tumors. *Mater. Chem. Front*. 2024, 8:3877–3897.

[71] Meng J, Wang L, Wang Q, Zou B, Ren S. Construction of artificial controllable aggregation trojan horse-like nanoplatform for enhanced NIR-II photothermal therapy. *ACS Appl. Mater. Interfaces* 2023, 15(4):4903–4910.

[72] Yu Y, Ni Z, Xu Y, Zhang L. Multi-functional AIE phototheranostic agent enhancing αPD-L1 response for oral squamous cell carcinoma immunotherapy. *Small* 2024, 20(48):e2405470.

[73] Zhou X, Hu Q, He C, Qian Y, Xu X, *et al.* Ferrocene-integrated hypericin self-assembly nanocomplex directs ferroptosis for enhanced cascade tumor photodynamic therapy and immune effects. *Chin. Chem. Lett*. 2026, 37(7):111645.

[74] Zhang W, Li X, Kang M, Zhang Z, Pei Y, *et al*. Anthraquinone-centered type I photosensitizer with aggregation-induced emission characteristics for tumor-targeted two-photon photodynamic therapy. *ACS Mater. Lett*. 2024, 6:2174−2185.

[75] Li X, Bai L, Wang Y, Zeng J, Wu W, *et al*. An anthracenyl-functionalized boron dipyrromethene based glutathione-responsive nanoplatform for efficient photodynamic therapy enhanced by perfluorooctanoic acid. *Small* 2026, 3:e73860.

[76] Nishiguch Y, Tani R, Nukaga S, Nishida R, Ikemoto A, *et al*. Pterostilbene induces apoptosis from endoplasmic reticulum stress synergistically with anticancer drugs that deposit iron in mitochondria. *Int. J. Mol. Sci*. 2024, 25(5):2611.

[77] Chen L, Zhao Y, Wang Y, Yang X, Zhao M. Achieving high-efficiency type I multimodal photosensitizers via a synergistic rigidity-flexibility strategy for hypoxia-resistant tumor therapy. *Small* 2026, 22:e13615.

[78] Song X, Huang H, Xia L, Jia W, Yang S, *et al*. Engineering 2D multienzyme-mimicking pyroptosis inducers for ultrasound-augmented catalytic tumor nanotherapy. *Adv. Sci. 2023*, 10(24):e2301279.

[79] Chen Y, Xiong T, Gu M, Li M, Chen X, *et al*. Pyrazolone-modified photosensitizers for precise cell membrane rupture to enhance cancer immunotherapy. *J. Am. Chem. Soc*. 2025, 147, 17915−17925.

[80] Xu X, Shabiti S, Zhang X, Zheng J, Liang N, *et al*. Membrane-anchoring clickable Iridium(III) nanosonosensitizer in situ evokes PANoptosis for augmented tumor sono-immunotherapy. *Nano Today* 2024, 56:102270.

[81] Liao S, Wang Y, Li Z, Zhang Y, Yin X, *et al*. A novel afterglow nanoreporter for monitoring cancer therapy. *Theranostics* 2022, 12(16):6883–6897.

[82] Huang L, Han G. Near infrared boron dipyrromethene nanoparticles for optotheranostics. *Small Methods* 2018, 2(9):1700370.

[83] Zhang Y, Ma D, Guo Y, Li B, Xue Y, *et al*. Ultra electron-donating segment dependence of NIR-II absorbing aza-borondipyrromethenes for photothermal/photodynamic phototherapy of breast cancer. *ACS Mater. Lett*. 2025, 7:3844−3852.

[84] Li X, Sun X, Chen H, Wang Y, Chen H, *et al*. Boron dipyrromethene-based nanotheranostic system for sonophotoassisted therapy and simultaneous monitoring of tumor immune microenvironment reprogramming. *ACS Nano* 2024, 18:18230−18245.

[85] Yang Z, Liu Y, Xie Z, Zheng M. Multifunctional boron-dipyrromethene platforms for disease diagnosis and therapy: advances in bioimaging, and phototherapeutics. *J. Photochem. Photobiol. C: Photochem. Rev*. 2026, 66:100739.

[86] Guo X, Tang B, Wu Q, Zhong W, Gong Q, *et al*. NIR-absorbing tetraphenylethene-containing bisBODIPY nanoplatforms demonstrate effective lysosome-targeting and combinational phototherapy. *ACS Appl. Mater. Interfaces* 2024, 16(32):41916–41926.

[87] Yu X, Duan Z, Yang H, Peng N, Zhao Z, *et al*. Supramolecular assemblies with aggregation-induced emission for in situ active imaging-guided photodynamic therapy of cancer cells. *Talanta* 2024, 280:126722.

[88] Shao L, Pan Y, Hua B, Xu S, Yu G, *et al*. Constructing adaptive photosensitizers via supramolecular modification based on pillararene host–guest interactions. *Angew. Chem. Int. Ed*. 2020, 59(29):11779–11783.

[89] Zhang Q, He M, Zhang X, Yu H, Liu J, *et al*. Tumor microenvironment activated chemodynamic–photodynamic therapy by multistage self-assembly engineered protein nanomedicine. *Adv. Funct. Mater*. 2022, 32(17):2112251.

[90] Upputuri P, Pramanik M. Photoacoustic imaging in the second near-infrared window: a review. *J. Biomed. Opt*. 2019, 24(4):040901.

[91] Liu Z, Wang Q, Qiu W, Lyu Y, Zhu Z, *et al.* AIE-active luminogens as highly efficient free-radical ROS photogenerator for image-guided photodynamic therapy. *Chem. Sci.* 2022, 13:3599–3608.